EXPERIMENTAL AND NUMERICAL STUDY ON DUCTILITY CAPACITY FOR SOLIDIFICATION CRACKING IN LASER BEAM WELDING

N. HABIBI*, A. GUMENYUK*, M. RETHMEIER**,*,***

**Bundesanstalt für Materialforschung und -prüfung (BAM), 12205 Berlin, Germany*
***Technische Universität Berlin, 10587 Berlin, Germany*
****Fraunhofer Institute for Production Systems and Design Technology IPK, 10587 Berlin, Germany*

DOI 10.3217/978-3-99161-089-2-028, license CC BY 4.0

ABSTRACT

Solidification cracking remains a critical challenge in laser beam welding, influenced by thermal, metallurgical, and mechanical factors. This study investigates the local conditions that contribute to this phenomenon in stainless steel 304 by measuring the temperature and strain evolution in the critical region. A custom measurement system was developed to estimate local temperature, strains, and strain rates, during controlled tensile weldability (CTW) experimental tests. This method enables a direct assessment of crack onset by applying a defined strain and strain rate during welding. To complement experimental findings, a parallel numerical study was conducted using a three-dimensional finite element (FE) model in ANSYS to trace the strain and stress development. The model incorporated sub-modeling of the critical area using predefined boundary conditions. This approach allows for the optimization of mesh size and time step to minimize numerical artifacts. Numerical results showed good agreement with experimental, in terms of level and distribution of temperature and strain, confirming the model's reliability. An iterative simulation approach was used to determine the critical strain conditions leading to crack initiation. These results were constantly compared with the experimentally observed data. This integrated method sheds light on the evolution of ductility and local straining conditions, enabling a more precise assessment of solidification cracking susceptibility. Corresponding author: andrey.gumenyuk@bam.de.

Keywords: Solidification Cracking, Laser Beam Welding, Finite Element Method

INTRODUCTION

Laser beam welding (LBW) is increasingly used in advanced manufacturing due to its precision, flexibility, and contactless operation, which enable it to be applied in aerospace, automotive, medical, and energy industries, where high weld quality is required. However, its effectiveness is often limited by solidification cracking, which can significantly reduce weld integrity and component safety [1].

Solidification cracking occurs in the mushy zone, the liquid-solid region between the advancing molten pool and the fully solidified weld metal. This region is bounded by the liquidus and solidus isotherms. In LBW, columnar dendritic grains typically dominate this zone unless grain refinement measures are applied [2]. As the weld cools and solidifies, the mushy zone undergoes thermal and solidification shrinkage. Because this contraction is restrained by the surrounding cooler base material, tensile stresses develop, which may separate the dendritic grains and initiate cracking [3]. Furthermore, the ductility of the material decreases significantly within this temperature range, and when the strain imposed on the mushy zone exceeds the available ductility, solidification cracking is likely to occur [4,5]. Several approaches have been developed to evaluate cracking susceptibility in LBW. Prokhorov [6] proposed the use of high-temperature ductility curves, from which the brittleness temperature range (BTR) can be derived. The BTR has been widely used to assess cracking susceptibility because larger BTR values indicate a higher risk of cracking [7].

Rappaz et al. [8] developed a microscopic model for hot tearing based on mass balance between thermal shrinkage and liquid feeding in the mushy zone, introducing RDG criteria based on critical strain rate at the end of solidification. Vernède and Dantzig [9] further elaborated on the mechanical behaviour of alloys during solidification using a mesoscale granular approach. Bellet et al. [10] proposed finite element approaches for thermomechanical simulation of hot tearing during arc welding of stainless steel, accounting for constitutive behaviour in the semi-solid state.

Experimental approaches determining the hot cracking behaviour of welded materials are based commonly on application of external loading of welding specimen combined with measurement of local strain close to the mushy zone or near to the solidification front.

In this regard, Shinozaki et al. [11] employed the U-type hot cracking test with in-situ observation during welding, which was improved in the further study [12] by higher quality imaging. Although this technique provided novel information about solidification cracking, it cannot capture the local strain history, which is essential for defining independent failure strains. To address these issues, promising works with optical measurement was conducted using optical flow technique [13,14]. However, this method only focuses on strains at the surface which is typically not the crack initiation site.

To overcome these challenges, the present work simulates solidification cracking through a controlled hot cracking experiment to provide deeper insight into this phenomenon. It is worth noting that significant contributions to thermomechanical modelling of hot tearing and solidification cracking have previously been made at the microscale. The present work operates at a larger, component-level scale, using a macroscopic FE model to predict crack onset conditions from experimentally applied boundary conditions, and is thus complementary to these microscale approaches.

EXPERIMENTAL PROCEDURE

The solidification cracking was studied on an austenitic stainless steel sheet of AISI 304 (1.4301) with a thickness of 1 mm through controlled tensile weldability (CTW) test, figure 1. This test developed at the Bundesanstalt für Materialforschung und -prüfung (BAM) in Berlin, is a hot-cracking assessment method. It uses a horizontal tensile testing setup with a 500 kN load capacity, capable of applying a planar tensile strain perpendicular to the welding direction at a controlled rate during welding. The test's principle involves adjusting the local strain rate near the mushy zone by systematically changing the overall applied strain rate (i.e., the cross-head speed). By observing whether cracks form or not, the test determines the critical global strain and strain rate that lead to cracking [15]. In this regard, the test performed in three stages: first, welding stabilization for 35 mm welding with no applied strain; second, the application of external loading at the defined global strain rate until the global strain was reached; and third, the global strain level was held at a constant value until the welding process was ended, when the total weld length is 100 mm. Afterwards, the possibility of hot cracking is investigated at the weld seam through X-ray radiography. As shown in figure 2, in this work, the CTW tests were performed at global strain rates of 0.02, 0.04, 0.06, and 0.08 s-1 at global strains of 0.02, 0.025, 0.03, and 0.035. Since this test forces the solidification cracking form at the centerline of the mushy zone, the track of cracking at the surface becomes easily possible. To measure the local distribution of temperature and strain, the set-up was equipped with a two-color pyrometer, a thermal SWIR [16] double-band camera, and a high-resolution sCMOS camera (the last one is not considered in this paper, detailed information is available in Ref. [17]). Figure 1. The welding parameters were selected to ensure fully penetration of the weld, i.e. a laser power of 1 kW and a constant welding speed of 1 m.min^{-1}, under the shielding gas of argon supplied through the lateral nozzle at the flow rate of 20 min^{-1}. For this study, the failure condition with strain of 0.025 and strain rate 0.06 s^{-1} was selected for the elaborate study through FE simulations.

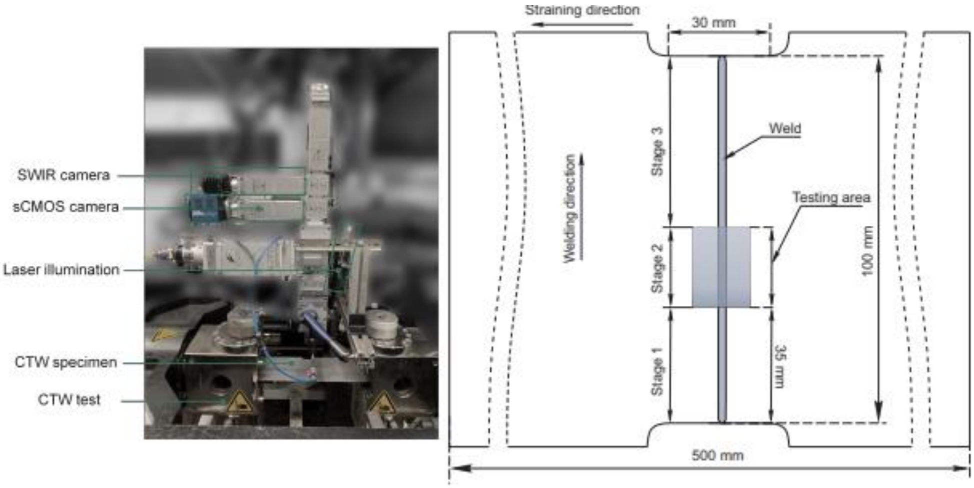

Fig. 1 (Left) The instrumented CTW-test set-up. (Right) The CTW specimen [14]

+	No crack
−	Crack
▨	N. A.

ε_{max} $\dot{\varepsilon}$ (s^{-1})	0.02	0.025	0.03	0.035
0.02	+	+	−	−
0.04	+	+	−	−−
0.06	+	−	−−	−−
0.08	+	−	−−	−−

Fig. 2 The weldability limits of AISI 304 through CTW tests

NUMERICAL PROCEDURE

Since cracking initiates in the center of thickness, the failure conditions cannot be defined precisely by the experimental set-up. Therefore, a three-dimensional FE model was developed using ANSYS Parametric Design Language (APDL). A full CTW specimen was designed with the adaptive meshing pattern to reduce the computation time. Thus, the fine elements of 0.185 mm × 0.185 mm × 0.2 mm were defined in the critical region, illustrated as the global-model in Fig. 3. The thermal and mechanical properties of the material were defined for a wide range of temperatures from 0 to 1500 °C, which were taken from the material library of Sysweld software [18], Fig. 4. Although the whole procedure modelled similar to the experiments, the laser beam was initially located not at the edge but 5 mm inside of the specimen, to escape the need for application transient thermal model at the process start and to eliminate any convergence problem.

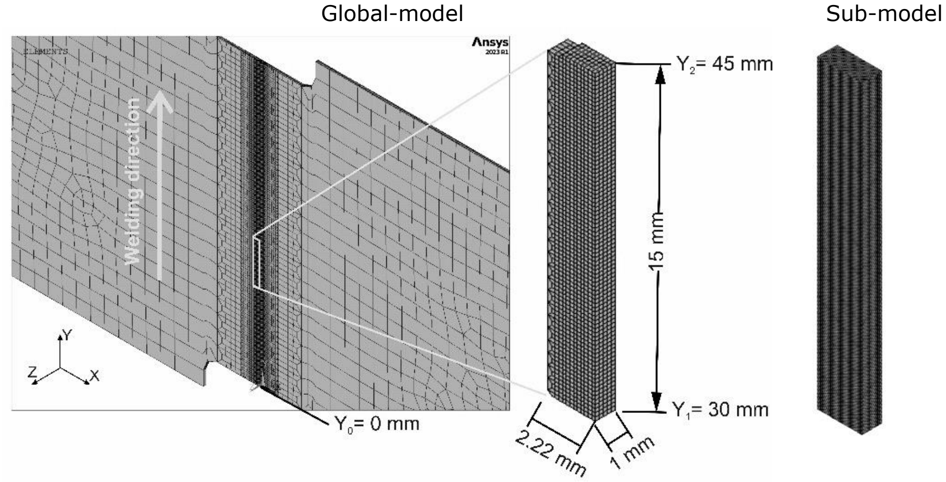

Fig. 3 The simulation model; (Left) Global-model; (Right) Sub-model

First, the thermal analysis was performed to determine the temperature history. Then, the temperature results were applied incrementally to the mechanical model to calculate stresses and strains. A step size of 0.01 s was defined for both simulations. For thermal model, an equivalent heat source with Dirichlet boundary condition was defined as the melt pool which had the homogeneous temperature of 1460 °C (liquidus temperature). Only the conductive mode was considered for heat transfer, and convection and radiation modes were neglected. The element type was defined as SOLID70 (3-D 8-Node Thermal Solid) [19].

As the chronological order of solidification in the weld seam has a significant influence on the nature and distribution of stresses within the BTR, the melt pool geometry was derived from CFD simulations from Ref. [20] and used as the equivalent heat source in the FEM model. In this regard, first the melt pool's height (z=1 mm) was divided into n planes (here n=20). At each plane, the geometry of the melt pool was approximated by two Lamé curves [21] one for approximation of the front shape (Eqn. 1) and one for the rear shape (Eqn. 2). The center was considered as the laser beam, which travelled along the weld line with the welding speed equal to the experimental tests.

$$\left|\frac{x}{a_f(z)}\right|^2 + \left|\frac{y}{b(z)}\right|^2 = 1 \tag{1}$$

$$\left|\frac{x}{a_r(z)}\right|^2 + \left|\frac{y}{b(z)}\right|^2 = 1 \tag{2}$$

where $a_f(z)$ and $a_r(z)$ are the semi-axes in x-direction for the front and rear parts and $b(z)$ is the semi-axis in y-direction. They were modeled as polynomials in the normalized depth $\xi = z/n$, as follows, in Eqn. 3 to 5:

$$a_f(z) = \sum_{i=0}^{7} c_{f,i}\xi^i \tag{3}$$

$$a_r(z) = \sum_{i=0}^{7} c_{r,i}\xi^i \tag{4}$$

$$b(z) = \sum_{i=0}^{7} c_{b,i}\xi^i \tag{5}$$

where $c_{f,i}$, $c_{r,i}$, and $c_{b,i}$ are the polynomial coefficients, which listed in Table 1 and the melt pool geometry is plotted in Figure 5.

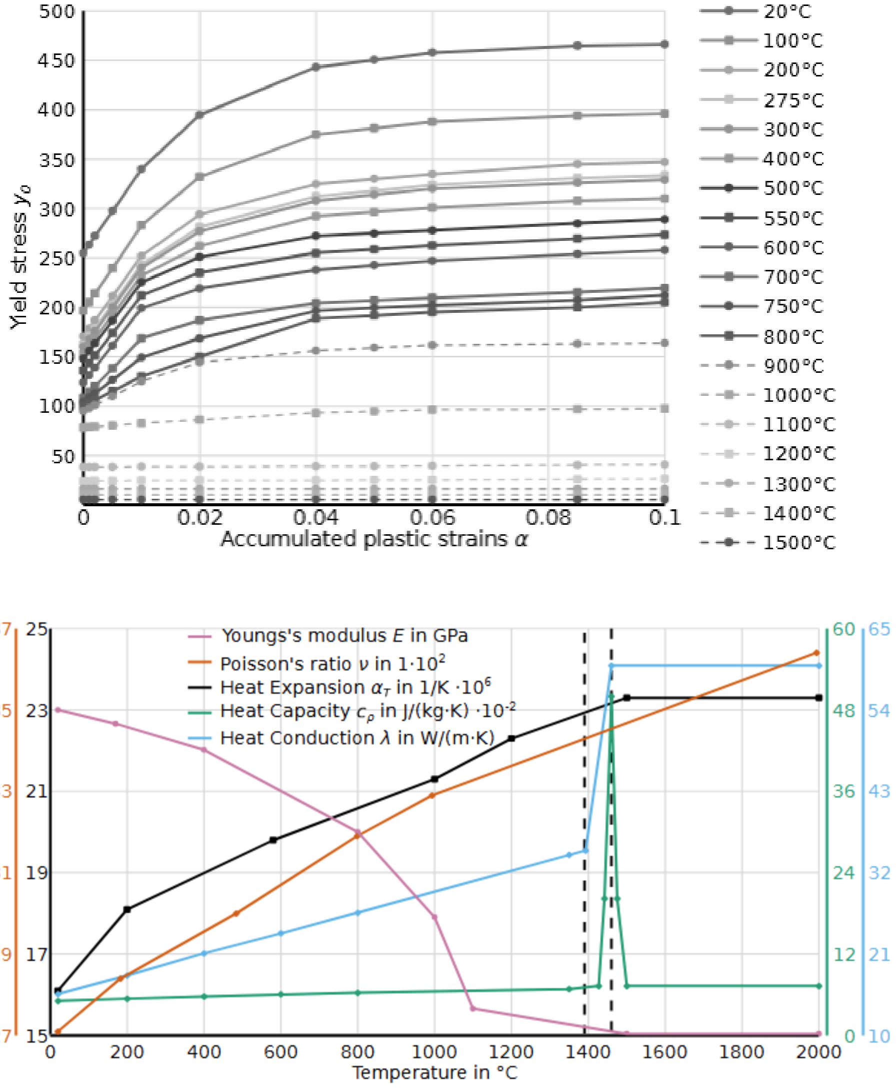

Fig. 4 The material temperature-dependent properties for the studied material taken from Sysweld software library [14,15]

Table 1. The polynomial coefficients for Lamé curves to create the melt pool geometry.

i	$c_{f,i}$	$c_{r,i}$	$c_{b,i}$
0	-3.6749	2.4598	1.1506
1	5.7263	-7.2852	-4.7981
2	1.4621	8.0229	6.5953
3	-6.4566	-3.9590	-3.8726
4	3.5316	0.7444	0.9514
5	-0.4531	-0.0835	0.2223
6	-0.0356	0.1167	-0.0676

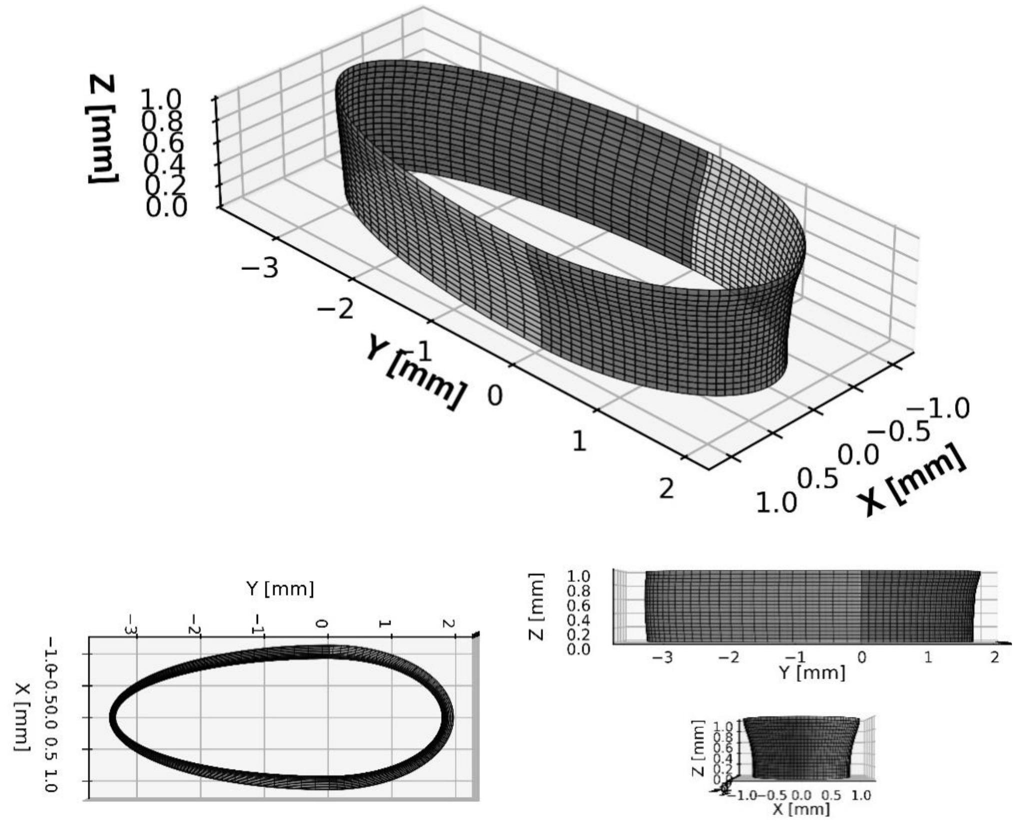

Fig. 5 The geometry of the melt pool

For the mechanical model, the CTW specimen was pulled from both sides to apply the strain of 0.025 and strain rate 0.06 s^{-1}. The element type was converted to SOLID186 (3-D 20-Node Structural Solid). The constitutive law employed in the mechanical analysis is a thermo-elasto-plastic formulation. The material is assumed to behave elastically according to Hooke's law, with temperature-dependent Young’s modulus and Poisson’s ratio. Plastic deformation is described using an isotropic hardening model with a von Mises yield criterion, where the yield stress is also a function of temperature. The total strain increment is decomposed into elastic, plastic, and thermal components. This formulation is appropriate for capturing the thermomechanical response of the material during the welding process, including the significant softening that occurs as the material approaches the solidus temperature.

Subsequently, a small section was cut out in order to use the sub-modelling technique with a finer element size of 0.05 mm × 0.05 mm × 0.05 mm. This yielded a total of 264,000 elements in a regular mesh, as shown in Fig. 3. One of the cut edges of the sub-model represents the symmetry plane of the specimen, where the correspondent boundary conditions were applied. Like the global-model, first the thermal simulation was performed with the thermal boundary conditions and then the temperature distribution was transferred to the mechanical simulations to simulate the effects of the mechanical boundary conditions. The thermal and mechanical boundary conditions for the cut edges (except of the symmetry plane) were taken from the global-model, as temperature and displacement increments.

Solidification crack was also considered in the sub-model, based on technological strength theory by Prokhorov [6]. Therefore, the mechanical boundary condition of the nodes located at the symmetry plane were released, and they were able to move freely as long as the total strain of the nodes were within brittle temperature range (BTR) and exceeded the critical strain value. The BTR and critical strain were iteratively selected to predict the closest size and location of the crack in comparison to the experimental results. Note that the employed cracking criterion was the critical total strain at the loading direction (x-direction).

RESULTS AND DISCUSSION

Fig. 6 shows the good agreement between the temperature distribution from the CFD simulation and the experimental results, as well as the results obtained by the FEM model. The X-ray radiography, Fig. 7, revealed while no crack initiated in the specimen for testing condition of $\varepsilon_{CTW} = 0.02$ and $\dot{\varepsilon}_{CTW} = 0.06\ s^{-1}$, a 2.4-mm crack exists for the testing condition of $\varepsilon_{CTW} = 0.025$ and $\dot{\varepsilon}_{CTW} = 0.06\ s^{-1}$.

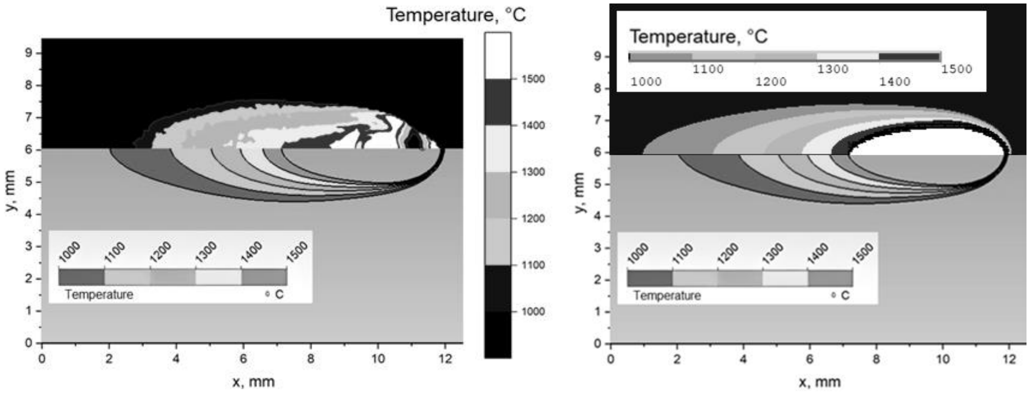

Fig. 6 The comparison of temperature distribution of the CFD simulation with (left) the experiment, and (right) the FEM simulation

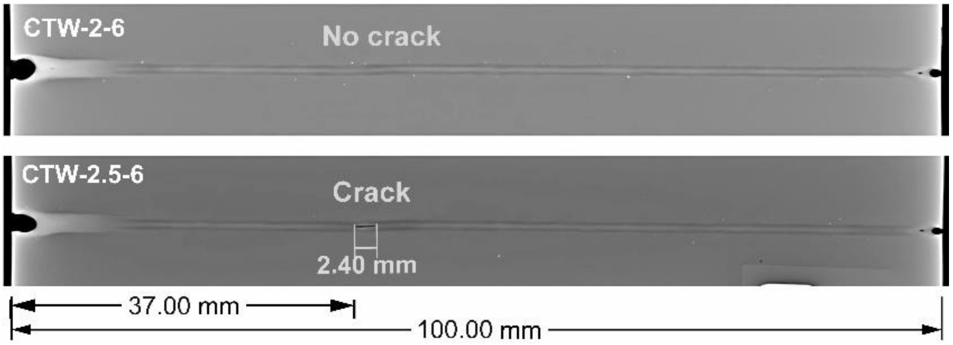

Fig. 7 Crack investigation by X-ray radiography for two CTW tests; (top) $\varepsilon_{CTW} = 0.02$ and $\dot{\varepsilon}_{CTW} = 0.06\ s^{-1}$ and (bottom) $\varepsilon_{CTW} = 0.025$ and $\dot{\varepsilon}_{CTW} = 0.06\ s^{-1}$

According to the iterative attempts, the brittle temperature range from 1360 to 1430 °C and the critical strain was chosen as 0.13 in the FE simulations led to cracking at the almost similar location and size in comparison to the experiments. Figure 8 illustrates the evolution of the crack. The distributions of temperature, displacement in the x-direction (i.e. the loading direction) and total strain in the x-direction were plotted at the begin of the external loading (t = 1.8 s), the initiation of the crack (t = 2.2 s), the end of the external loading (t = 2.22 s) and the end of the crack growth (t = 2.36 s). The results imply that cracking initiated at $\varepsilon_{CTW} = 0.024$ at the stage 2 of the test and continued even after the external loading is stopped, which corresponds to the stage 3 of the test. To better understand the reason, thermal, mechanical and total strains at x-direction are illustrated in Fig. 9 at the crack initiation, the end of loading, the frame after the end of loading, the end of crack growth, and the next frame of the end of cracking. It is noted that, in a thermomechanical problem, mechanical strain also arises from thermal gradients and structural constraint; the term “mechanical strain” used throughout this work refers specifically to the strain component driven by the externally applied loading, to distinguish it from the thermally-induced strain component. Here, the focus was only strains at x-direction, although it might not be written each time. To improve the illustration, the specimen is selected at the YZ plane from Y = 37 mm to 41 mm, and the crack elements are deleted from the display. The size and location of the crack can also be seen there. The results show that after the external loading was stopped, the mechanical strain remained constant, as expected. Only the BTR was moving with the laser beam which is associated with the local growth of the thermal strain up to 0.03. Whenever a node was in the BTR and the stored mechanical strain plus the thermal strain, i.e. the total strain, reached 0.13, the critical condition was satisfied, and the mechanical boundary condition was released at that node to form the cracking. While if the stored mechanical strain for a node was small and its sum with the thermal strain did not reach the threshold, the cracking did not occur. Note that, during the external loading, the mechanical strain was higher when the temperature is higher. Therefore, when the loading was stopped, the stored mechanical strain was significantly lower for the elements in front of the laser beam than the ones located behind it.

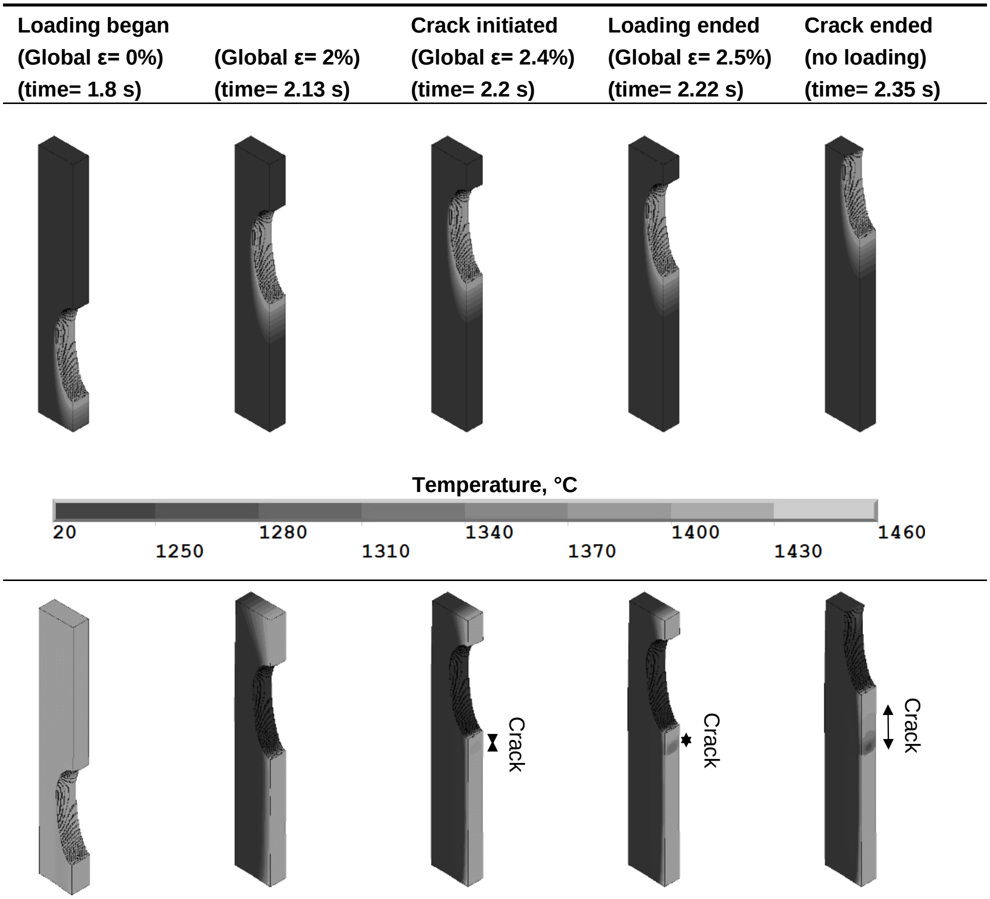

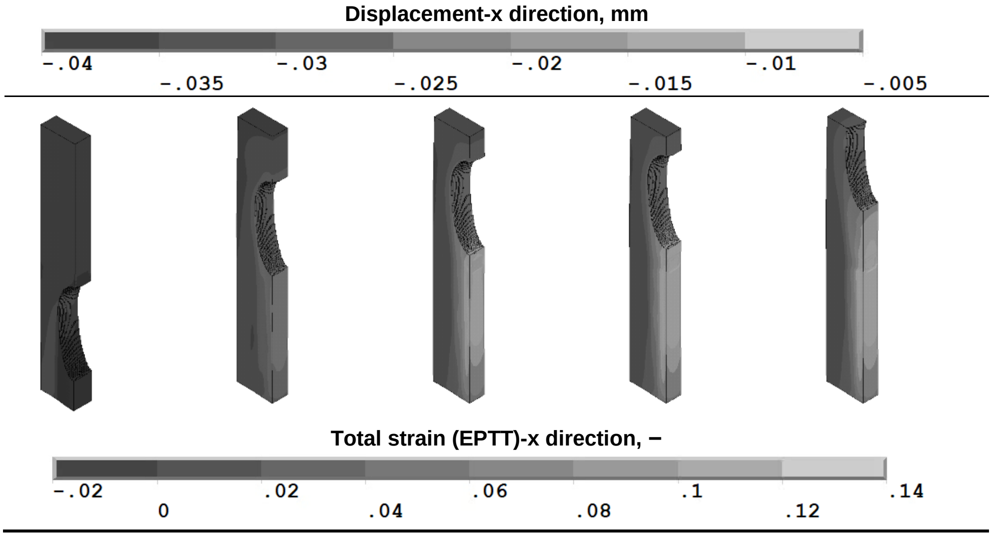

Fig. 8 Distribution of temperature, displacement, and total strain along x-direction (loading direction). The elements for the weld pool were removed from the display.

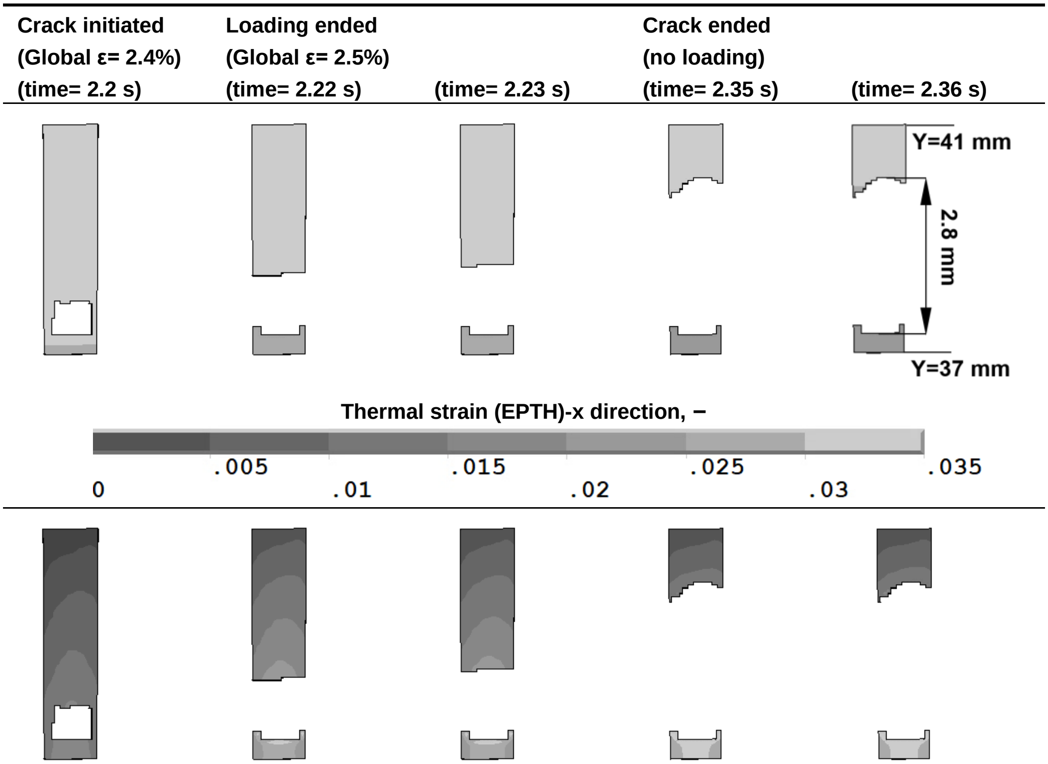

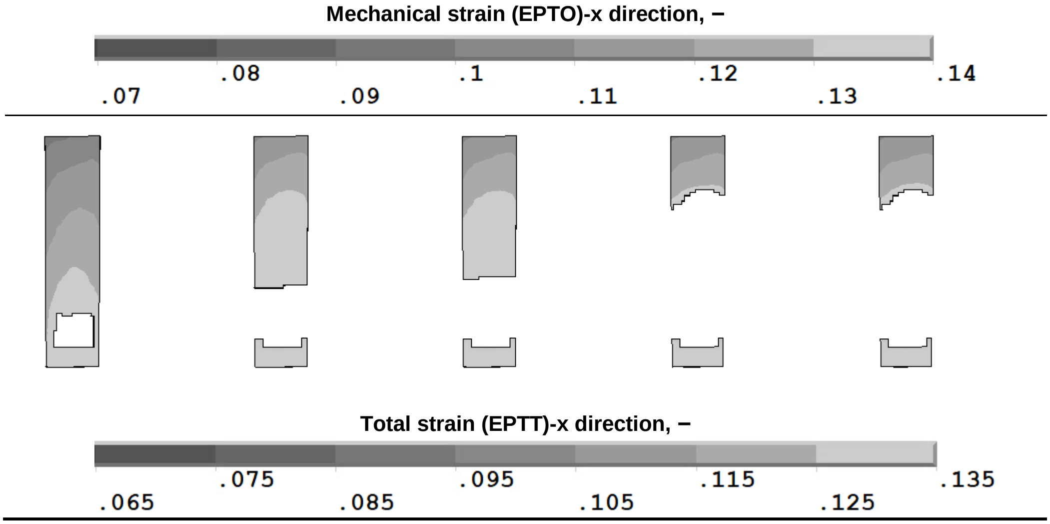

Fig. 9 Thermal, mechanical, and total strain evolution at x-direction. It is shown at YZ-plane from y=37 to 41 mm.

CONCLUSION

The sensitivity of AISI 304 to the solidification cracking was evaluated through CTW test. The systematic experimental approach provided valuable information regarding the crack and no crack conditions for the applied external loading. The FEM simulation was used for the elaborate study, which revealed for this material the sum of the mechanical and thermal strains at the loading direction was responsible for cracking i.e. the total strain in the cracking criterion. When this variable reached its threshold at the critical temperature condition (BTR) cracking happened. By stopping the external loading, some mechanical strain stored at the material, which could lead to the further crack growth, if its value plus the thermal strain component still satisfied the critical cracking condition.

ACKNOWLEDGEMENTS

This research is funded by the Deutsche Forschungsgemeinschaft (DFG, German Research Foundation) - Project ID 434946896, within the research unit FOR 5134: ‘Solidification Cracks during Laser Beam Welding: High Performance Computing for High Performance Processing’.

References

[1] J. C. LIPPOLOLD: *Welding metallurgy and weldability*, First ed., M. John Wiley & Sons Inc, pp. 85-94, 2015.

[2] T. KOSEIKI, H. INOUE, ET AL.: *Nippon Steel Technology Report*, No. 65, April 1995.

[3] M. C. FLEMINGS: *Solidification Processing*, McGraw-Hill, New York, pp. 251-255, 1974.

[4] S. A. DAVID, C. L. WHITE and V. P. KUJANPAA: 'Formation of Hot Cracks in Austenitic Stainless Steel Welds - Solidification Cracking', *Weld Research Supplement*, No. 65, pp. 203-212, 1986.

[5] K. KADOI, A. FUJINAGA, M. YAMAMOTO and K. SHINOZAKI: 'The effect of welding conditions on solidification cracking susceptibility of type 310S stainless steel during laser welding using an in-situ observation technique', *Weld World*, Vol. 57, pp. 383-390, 2013.

[6] N. N. PROKHOROV: 'Resistance to hot tearing of cast metals during solidification', *Russian Castings Production*, Vol. 2, No. 2, pp. 172-175, 1962.

[7] G. J. DAVIES and J. G. GARLAND: 'Solidification Structures and Properties of Fusion Welds', *International Materials Reviews*, Vol. 20, pp. 83-108, 1975.

[8] M. RAPPAZ, J.-M. DREZET and M. GREMAUD: 'A new hot-tearing criterion', *Metallurgical and Materials Transactions A*, Vol. 30, No. 2, pp. 449-455, 1999.

[9] S. VERNÉDE, J. DANTZIG and M. RAPPAZ: 'A mesoscale granular model for mechanical behaviour of alloys during solidification', *Acta Materialia*, Vol. 57, pp. 1554-1569, 2009.

[10] M. BELLET, G. QIU and J. CARPREAU: 'Comparison of two hot tearing criteria in numerical modelling of arc welding of stainless steel AISI 321', *Journal of Materials Processing Technology*, Vol. 230, pp. 141-152, 2016.

[11] P. WEN, K. SHINOZAKI, M. YAMAMOTO, Y. SENDA, T. TAMURA and N. NEMOTO: 'In-situ Observation of Solidification Cracking of Laser Dissimilar Welded Joints', *Quarterly Journal of JWS*, Vol. 27, No. 2, pp. 134-138, 2009.

[12] S. YANG, T. ITO, K. SHINOZAKI and M. YAMAMOTO: 'The effect of welding and strain conditions on the susceptibility to solidification cracking of a fully austenitic stainless steel', in *77th IIW Annual Assembly and International Conference*, Rhodes, Greece, July 7-12, 2024.

[13] W. HUO, N. BAKIR, A. GUMENYUK, M. RETHMEIER and K. WOLTER: 'Strain prediction using deep learning during solidification crack initiation and growth in laser beam welding of thin metal sheets', *Applied Sciences*, Vol. 13, No. 5, p. 2930, 2023.

[14] W. HUO, N. BAKIR, A. GUMENYUK, M. RETHMEIER and K. WOLTER: 'Detection of solidification crack formation in laser beam welding videos of sheet metal using neural networks', *Neural Computing and Applications*, Vol. 35, No. 34, pp. 24315-24332, 2023.

[15] N. BAKIR, A. GUMENYUK and M. RETHMEIER: 'Determination of critical local straining conditions for solidification cracking at laser beam welding by experimental and numerical methods', *PAMM*, Vol. 24, No. 2, p. e202400020, 2024.

[16] A. GUMENYUK, N. BAKIR and M. RETHMEIER: 'Two-colour thermography for measurement of temperature distribution in laser beam welding', *Procedia CIRP*, Vol. 124, pp. 468-471, 2024.

[17] T. BEVILACQUA, A. GUMENYUK, N. HABIBI, P. HARTWIG, A. KLAWONN, M. LANSER, M. RETHMEIER, L. SCHEUNEMANN and J. SCHRÖDER: 'Large-scale thermo-mechanical simulation of laser beam welding using high-performance computing: a qualitative reproduction of experimental results', *arXiv preprint*, arXiv:2503.09345, 2025.

[18] ESI GROUP: *Sysweld Material Database*, Software, Paris, France, 2009.

[19] ANSYS, INC.: *Ansys Mechanical APDL reference manual (2023 R2)*, Software, Canonsburg, Pennsylvania, US, 2023.

[20] P. HARTWIG, N. BAKIR, L. SCHEUNEMANN, A. GUMENYUK, J. SCHRÖDER and M. RETHMEIER: ‘A physically motivated heat source model for laser beam welding’, *Metals*, Vol. 14, No. 4, p. 430, 2024.

[21] A. ARTINOV, V. KARKHIN, N. BAKIR, X. MENG, M. BACHMANN, A. GUMENYUK and M. RETHMEIER: ‘Lamé curve approximation for the assessment of the 3D temperature distribution in keyhole mode welding processes’, *Journal of Laser Applications*, Vol. 32, No. 2, 2020.